ACTA CHEMICA IASI, **34_1**, 166-184 (2026)
DOI: 10.47743/achi-2026-1-0006

Article

EFFECTS OF B-SITE CATION SUBSTITUTION ON THE STRUCTURAL, DIELECTRIC, AND CATALYTIC PROPERTIES OF $Sr_2Fe_{1-x}Ta_{1+x}O_6$ DOUBLE PEROVSKITES ($0 \leq x \leq 0.5$)

Gorodea Ioana Aurelia*

Department of Chemistry, Alexandru Ioan Cuza University of Iasi, 11 Carol I Bd, Iasi 700506, Romania

Abstract: $Sr_2Fe_{1-x}Ta_{1+x}O_6$ ($0 \leq x \leq 0.5$) double perovskites were synthesized by a solid-state reaction at 1300 °C in air. The influence of B-site cation substitution and anti-site disorder on the structural, dielectric, and catalytic properties was investigated. X-ray diffraction (XRD) analysis, combined with Rietveld refinement showed that all compositions crystallize in an orthorhombic structure. Infrared (IR) spectroscopy in the 4000–400 cm^{-1} range supported these structural results. The dielectric behavior was evaluated from resistivity measurements over the frequency range 10–10^6 Hz, indicating a systematic dependence of permittivity and dielectric loss on composition (x). The performance of the materials in γ-ray-induced water radiolysis was evaluated using the radiolytic hydrogen yield (G_{H_2}).The results show that increasing Ta content enhances radiolysis performance, with x = 0.5 exhibiting the highest hydrogen yield.

***Keywords*:** double perovskites; B-site substitution; solid-state synthesis; X-ray diffraction; dielectric properties; water splitting

* Gorodea Ioana, *e-mail:* gorodea@uaic.ro

Introduction

The crystal structures of double perovskite based on transition metal oxides have been extensively studied due to their ability to crystallize in all seven crystal systems, depending on the nature of the A and B cations, their ordering on the octahedral sites and the synthesis method employed. This structural versatility leads to a wide range of physical properties, making perovskites one of the most important classes of materials for industrial and scientific applications.

It is well established that the most important factors affecting the arrangement of cations at the B site are ionic charge, ionic radius, and electronic configuration. These factors can lead to structures exhibiting ideal ordering, partial ordering, local disorder, or complete disorder. In recent years, particular attention has been paid to the influence of the charge difference between metal cations, which plays a key role in stabilizing ordered structures. The B-site ordered double perovskite structure of $A_2B'B''O_6$ compounds is derived from the single perovskite ABO_3 structure, in which the octahedral B site is occupied by two different metal cations, B′ and B″. Cation ordering arises from differences in charge and/or ionic radius between B-site cations, leading to preferential ionic arrangements in ABO_3-type perovskites.[1] A high degree of B-site ordering typically requires a significant charge difference between B′ and B″ cations; for instance, B′(I)–B″(VII) and B′(II)–B″(VI) systems exhibit nearly perfect ordering, whereas B′(III)–B″(V) systems tend to show partial ordering.[2]

Complex tantalum oxides have attracted considerable interest due to their photocatalytic activity, ferroelectric behaviour, and dielectric properties.[3-5] These mixed perovskite oxides have a wide range of applications, particularly as dielectric materials.[6,7] The dielectric constant

depends strongly on synthesis conditions, while factors such as porosity, crystallite size, and ionic conductivity can decrease the dielectric constant and increase dielectric losses. Sr_2FeTaO_6 is a typical double perovskite known for its chemical and thermodynamic stability, while the multivalence of Fe facilitates oxygen ion migration. Double perovskites have also been reported to enhance water radiolysis due to their unique structure and large surface area.[8]

In recent years, double perovskite oxides have attracted increasing attention for applications in energy conversion and environmental remediation, particularly in photocatalysis, water splitting, and radiation-induced processes. Their functional properties are strongly influenced by the interplay between crystal structure, cation ordering, and defect chemistry. In particular, the presence of mixed-valence transition metals and oxygen vacancies plays a crucial role in charge transport, polarization mechanisms, and catalytic activity. Among these materials, Fe-based double perovskites are especially promising due to the variable oxidation states of iron, which facilitate electron transfer processes and enhance catalytic performance. Furthermore, substitution at the B site provides an effective strategy to tailor the electronic structure and defect concentration, thereby tuning both dielectric and catalytic responses. Despite numerous studies on tantalum-based perovskites, the combined effect of cation substitution and anti-site disorder on dielectric behaviour and γ-radiation-induced catalytic activity remains insufficiently explored.

For double perovskites with the general formula A_2AlTaO_6 (A = Ca, Sr, Ba), the role of A-site cations in determining structural, dielectric, and catalytic properties has been investigated.[9] It has been shown that a decrease in the average ionic radius of the A-site cations induces a

structural transition from cubic to monoclinic symmetry. Additionally, the relative permittivity and dielectric loss vary systematically with the size of the A-site cation. The perovskite Ca_2AlTaO_6 exhibits a more distorted structure and a higher concentration of anion vacancies, which leads to enhanced performance in γ-ray-induced water radiolysis.

Therefore, the present study aims to synthesize $Sr_2Fe_{1-x}Ta_{1+x}O_6$ ($0 \leq x \leq 0.5$) using the conventional solid-state method and to provide a systematic investigation of the correlation between cation substitution, structural ordering, and functional properties, with particular emphasis on dielectric response and γ-ray-assisted catalytic activity. Although increasing substitution does not significantly improve structural ordering, enhancements in dielectric and catalytic performance are observed.

Results and discussion

The double perovskite series $Sr_2Fe_{1-x}Ta_{1+x}O_6$ ($0 \leq x \leq 0.5$), synthesized via a solid-state reaction at 1300 °C for 48 h, was analyzed using X-ray diffraction (XRD). Measurements were performed at room temperature on a SHIMADZU XRD-6000 diffractometer with a Ni filter and Cu Kα radiation (λ = 1.5418 Å), a step size of 0.02°, and a counting time of 1 s per step over a 2θ range of 20–80°. The corresponding XRD patterns are presented in Figure 1. All profiles exhibit sharp, well-defined peaks, indicating the high crystallinity of the prepared materials and confirming the formation of the double perovskite phase without detectable secondary phases.

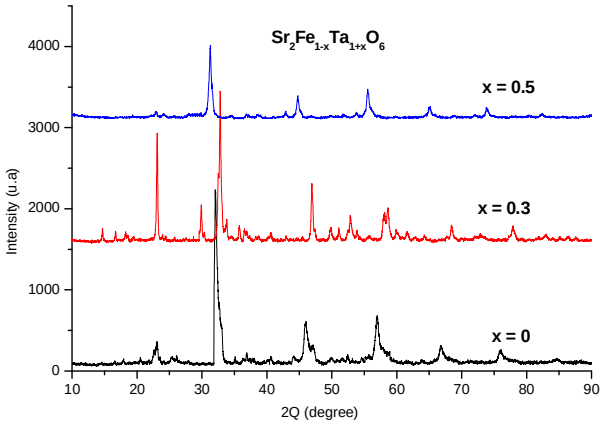

Figure 1. X-ray diffraction patterns $Sr_2Fe_{1-x}Ta_{1+x}O_6$ ($0 \leq x \leq 0.5$) sintered at 1300˚C for 48 hours.

For the composition with x = 0, all diffraction peaks can be indexed to an orthorhombic unit cell with the *Pbnm* space group (see Figure 2). Structural parameters, including lattice constants, unit cell volume, and tolerance factor (t), were calculated using the Structure Prediction Diagnostic Software (SPuDS)[10] and are summarized in Table 1. The most intense reflections can be indexed to characteristic planes of the double perovskite structure, consistent with the formation of the intended phase.

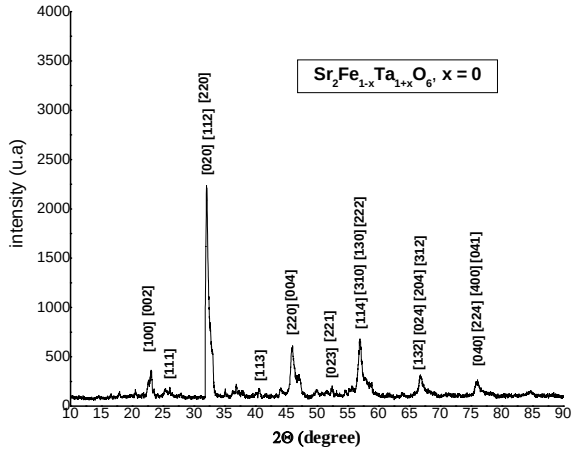

Figure 2. X-ray diffraction patterns Sr_2FeTaO_6.

Table 1. Crystallographic data calculated from SPuDS for powder $Sr_2Fe_{1-x}Ta_{1+x}O_6$ ($0 \leq x \leq 0.5$), sintered at 1300 °C.

Compound	Space group	T (tolerance factor)	Cell-parameter (Å)	V(Å^3)
$Sr_2Fe_{1-x}Ta_{1+x}O_6$ x=0	Pbnm ortorombic	t = 0.983	a = 5.6204 Å, b = 5.6161 Å, c = 7.9266 Å	271 Å^3
$Sr_2Fe_{1-x}Ta_{1+x}O_6$ x=0.3	Pbnm ortorombic	t = 0.984	a = 5.7804 Å, b = 5.7861 Å, c = 8.1700 Å	273 Å^3
$Sr_2Fe_{1-x}Ta_{1+x}O_6$ x=0.5	Pbnm ortorombic	t = 0.984	a = 5.7704 Å, b = 5.7761 Å, c = 8.1600 Å	272 Å^3

Cation substitution does not lead to a high degree of ordering between Fe and Ta at the B and B′ sites. Consequently, the (111) superlattice reflection, which is indicative of B-site ordering, is absent in the XRD pattern for x = 0.5. Similar disorder has been observed in related systems, such as Nb-containing double perovskites. This behavior can be attributed to the relatively small differences in ionic radius and charge between Fe^{3+} and Ta^{5+}, which reduce the driving force for long-range ordering. Electrostatic interactions and local structural constraints promote a random distribution of cations at the B sites, leading to structural distortions that stabilize orthorhombic or tetragonal phases.

The tolerance factor was found to increase slightly with increasing substitution, exhibiting only minor variation. Since $t < 1$ for all compositions, the perovskite structure adopts a lower-symmetry configuration rather than the ideal cubic form. These observations suggest that the structural stability of $Sr_2Fe_{1-x}Ta_{1+x}O_6$ is governed more strongly by the cation charge distribution than by purely geometric effects. The slight

peak shifts observed with increasing x further indicate modest variations of the lattice parameters due to cation substitution.

The lattice constants (a, b, and c) and unit cell volume show a slight increase with increasing x, reflecting the incorporation of larger Ta^{5+} ions in place of Fe^{3+}. The FeO_6 and TaO_6 octahedra exhibit minor tilting and distortion, consistent with the orthorhombic symmetry of all compositions.[11] The absence of the (111) superlattice reflection in samples with x = 0.5 indicates partial B-site disorder, which has been observed previously in related double perovskites such as Sr_2FeMoO_6. This disorder, together with subtle lattice distortions, is expected to affect dielectric polarization, charge transport, and catalytic efficiency under γ-radiation.

FT-IR spectra of the $Sr_2Fe_{1-x}Ta_{1+x}O_6$ ($0 \leq x \leq 0.5$) were recorded over the 4000–400 cm^{-1} range using a JASCO 660 PLUS spectrophotometer to complement the structural analysis. The samples were mixed with KBr at a mass ratio of 0.04:1 and pressed into pellets 0.5–0.75 mm thick and 13 mm in diameter under a pressure of 0.3 GPa in air.

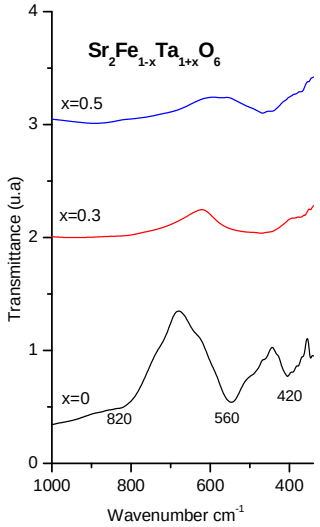

Figure 3. FTIR spectra of $Sr_2Fe_{1-x}Ta_{1+x}O_6$ ($0 \leq x \leq 0.5$) sintered at 1300°C.

All spectra exhibit three characteristic absorption bands between 850 cm^{-1} and 400 cm^{-1}, confirming the formation of the perovskite phase.[12] A strong high-energy band centred at ~660 cm^{-1} is assigned to the antisymmetric stretching vibrations of TaO_6 octahedra, while a band at ~840 cm^{-1} corresponds to their symmetric stretching vibrations. A prominent band at ~450 cm^{-1} is attributed to the deformation modes of $Ta(Fe)O_6$ octahedra (Figure 3).

Variations in the FT-IR spectra arise from differences in crystal symmetry induced by Fe-to-Ta substitution. In Sr_2FeTaO_6 (x = 0), which exhibits orthorhombic symmetry, a weak band at 820 cm^{-1} corresponds to the symmetric stretching vibrations of TaO_6 octahedra, while a medium-intensity band at 560 cm^{-1} reflects antisymmetric stretching. The medium-to-weak band at 420 cm^{-1} is assigned to stretching vibrations of FeO_6 octahedra.

For $Sr_2Fe_{1-x}Ta_{1+x}O_6$ ($0 \leq x \leq 0.5$), the disappearance of the ~800 cm^{-1} band indicates that symmetric stretching of TaO_6 octahedra is suppressed, consistent with increased B-site disorder. Antisymmetric stretching bands show a decrease in intensity, occasional splitting (observed for x = 0.3), and a progressive shift toward lower wavenumbers with increasing x, indicative of slight elongation or compression of FeO_6 and TaO_6 octahedra. The low-energy bands in the 300–400 cm^{-1} range may also split, corresponding to deformation modes of FeO_6 polyhedra.

These observations confirm that Fe-to-Ta substitution does not enhance cation ordering at the B and B′ sites. Instead, the resulting compounds exhibit a lower degree of symmetry and local lattice distortions. Such structural modifications are expected to influence dielectric

polarization and catalytic activity by altering local bonding environments and electron distribution.

The variation of the dielectric constant with frequency shows a typical dielectric dispersion attributed to Maxwell–Wagner-type interfacial polarization [13], in agreement with Koop's phenomenological theory.[14] This interfacial polarization arises from charge accumulation at grain boundaries and other inhomogeneities within the ceramic matrix, which dominate at low frequencies and diminish as the applied field frequency increases.[15]

Analysis of the dielectric data indicates that the degree of B-site cation substitution significantly influences the electrical properties. In particular, $Sr_2Fe_{1-x}Ta_{1+x}O_6$ with x = 0.5 exhibits the lowest dielectric losses among all substituted samples and a permittivity within the range characteristic of high-quality dielectric materials. The observed decrease in dielectric losses correlates with structural distortions and partial B-site disorder, as confirmed by XRD and FT-IR analyses.

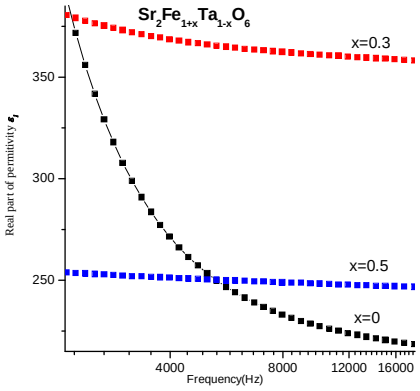

Figure 4. The real part variation of the dielectric constant with frequency for $Sr_2Fe_{1-x}Ta_{1+x}O_6$ ($0 \leq x \leq 0.5$).

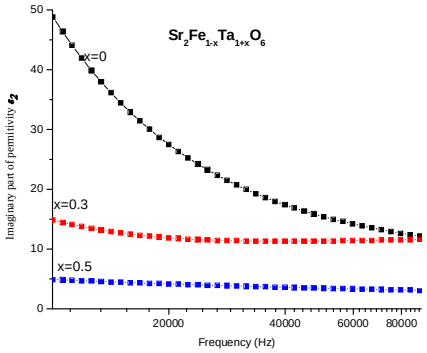

Figure 5. The imaginary part variation of the dielectric constant with frequency for $Sr_2Fe_{1-x}Ta_{1+x}O_6$ ($0 \leq x \leq 0.5$).

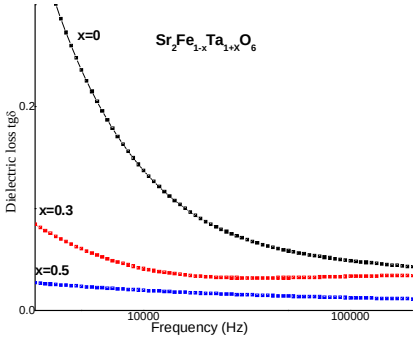

Figure 6. The dielectric loss function on frequency for $Sr_2Fe_{1-x}Ta_{1+x}O_6$ ($0 \leq x \leq 0.5$).

Figures 4 and 5 show that both the real (ε′) and imaginary (ε″) components of the dielectric constant decrease with increasing frequency, eventually reaching nearly constant values at high frequencies. The dielectric loss function ($\tan\delta$) of $Sr_2Fe_{1-x}Ta_{1+x}O_6$ ($0 \leq x \leq 0.5$) decreases with increasing frequency (Figure 6), showing maximum dispersion at low frequencies due to interfacial polarization and defect-related charge accumulation, and gradually stabilizes at high frequencies, reflecting the intrinsic dielectric response of the perovskite lattice.

The observed changes in dielectric behavior can be explained by the structural disorder caused by Fe/Ta substitution at the B-site. This disorder

leads to local variations in charge distribution and lattice distortions, which affect the polarization process. In addition, charge accumulation at grain boundaries contributes to space-charge polarization. The distortion of $(Fe/Ta)O_6$ octahedra and changes in bond lengths further influence the dielectric response. These effects together are responsible for the observed frequency-dependent dielectric relaxation.

All materials exhibit normal dielectric behavior, and the dielectric properties remain stable over the measured frequency range, indicating good structural and thermal stability. The dielectric constant and loss are influenced by cation substitution, crystal structure, porosity, and chemical homogeneity of the compounds. Similar behavior has been reported for other double perovskites, such as Sr_2FeMoO_6 and Ca_2AlTaO_6, where B-site substitution affects dielectric properties through lattice distortions and defect-induced polarization.[16] These results highlight the critical role of B-site composition in tuning dielectric performance and suggest that $Sr_2Fe_{1-x}Ta_{1+x}O_6$ (x = 0.5) is a promising candidate for high-frequency dielectric applications due to its low losses and stable permittivity.

The radiolysis performance of the double perovskites $Sr_2Fe_{1-x}Ta_{1+x}O_6$ (x = 0.5) in γ-ray-induced water splitting was investigated for the first time. Irradiation was performed using a ^{60}Co source with an activity of 3×10^4 Ci and a dose rate of 8.3 kGy/h, simulating the conditions of highly active radioactive waste (10^8–10^9 Ci) resulting from the reprocessing of spent nuclear fuel.

Radiolysis products, including stable species and intermediates, were analyzed by mass spectrometry. For sample preparation, varying amounts of each catalyst were placed in 30 mL glass vials, to which 5 mL of double-distilled water was added. Each vial was tightly sealed with a rubber

stopper and coated with paraffin to prevent the release of gaseous radiolysis products. The vials were then γ-irradiated under different experimental conditions and dose rates at IFIN-Bucharest.

The radiolysis products were measured using a Hiden Analytical mass spectrometer, connected to the irradiated samples via a custom metallic capillary interface.

Radiation-induced water splitting using perovskites has received considerable attention as a potential clean and renewable source of hydrogen fuel. An ideal catalyst should not react with the solvent and must be resistant to the effects of light or nuclear radiation.[17] Compounds of the formula $Sr_2Fe_{1-x}Ta_{1+x}O_6$ ($0 \leq x \leq 0.5$) have been employed, for the first time, as catalysts in water radiolysis.

It is generally known that the radiolysis of water leads to the formation of different chemical species, such as H_2, O_2, H_2O_2, HO•, O and HO_2• via a number of reactions outlined below, as:

$$\sim\sim\rightarrow H_2O \rightarrow H_2O^* \rightarrow H\bullet + HO\bullet \quad (1)$$

$$\sim\sim\rightarrow H_2O \rightarrow H_2O^+ + e^- \quad (2)$$

$$H_2O + e\text{-} \rightarrow H_2O^- \quad (3)$$

$$H_2O^+ + H_2O^- \rightarrow 2H_2O^* \rightarrow 2H^{\cdot} + 2HO^{\cdot} \quad (4)$$

$$H\bullet + H\bullet \rightarrow H_2 \quad (5)$$

$$H\bullet + O \rightarrow HO\bullet \quad (6)$$

$$HO\bullet + HO\bullet \rightarrow HO_2\bullet + H\bullet \quad (7)$$

$$HO_2\bullet + HO_2\bullet \rightarrow H_2O_2 + O_2 \ldots \quad (8)$$

$$H_2O_2 + HO\bullet \rightarrow HO_2\bullet + H_2O \quad (9)$$

$$H\bullet + O_2 \rightarrow HO_2\bullet \quad (10)$$

Radiolytic yield of hydrogen, G_{H_2} (number of transformed or appeared molecules for 100 eV absorbed energy, by c-ray irradiation) was calculated using a formula deduced from Henglein expression

$$G_{H_2} = \frac{\text{b Ix}}{D\ t\ \rho\ Iet} 9.66.10^6$$

where:

D·t = Da means absorbed dose (1 J/kg or $6.24 \cdot 10^{15}$ eV/g);

ρ = the density of irradiated material (g/cm3);

b = hydrogen amount determined from the calibration of mass spectrometer (mole H_2/1 kg H_2O);

Iet = is peak intensity value of molecular hydrogen resulted from the mass spectrometer calibration reaction;

Ix = is peak intensity value of molecular hydrogen resulted from the catalyzed water radiolysis.

Several reactive species, including H_2, HO_2•, HO_2^-, and H_2O_2, were identified in the mass spectra; however, the radiolytic yield was quantified exclusively for molecular hydrogen.[18] The experimental findings, as well as the catalytic efficiency in the water radiolysis process, were evaluated based on the radiolytic yield values of molecular hydrogen under various operating conditions (Figure 7 and Figure 8). The results indicate that the radiolytic yield of H_2 increases with increasing absorbed dose at a fixed catalyst amount, as well as with increasing catalyst (perovskite) mass at a constant dose. Exposure to gamma irradiation induces the radiolytic decomposition of water, leading to enhanced hydrogen production. In the presence of the catalyst, the radiolytic yield of H_2 (G_{H_2}) exceeds the value obtained for pure water radiolysis (0.43) under identical irradiation conditions.

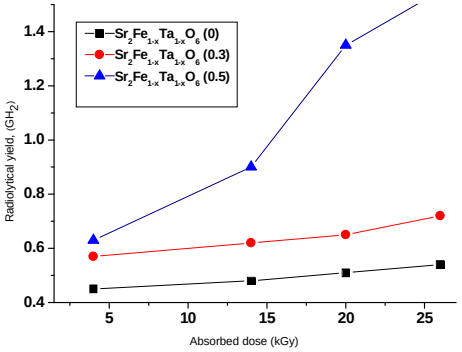

Figure 7. Radiolytic yield vs absorbed dose.

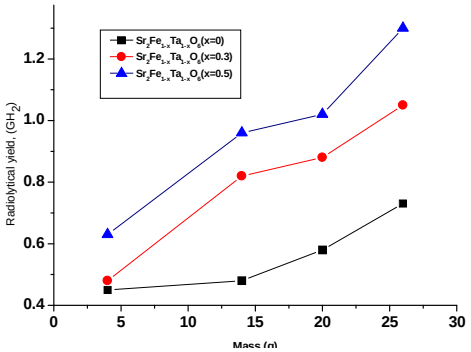

Figure 8. Radiolytic yield vs catalysts mass.

Perovskite oxides typically contain a high concentration of oxygen vacancies, resulting from cation stoichiometry and valence.[19,20] Neutral water molecules are expected to occupy these oxide vacancies. Anionic vacancies $V_{O..}$ act as Lewis acids, while water molecules act as Lewis bases:

$$^{V}{}_{O..} + \mathbf{O}_{Ox} + H_2O \leftrightarrow 2\ OH_O$$

The stoichiometric changes that occur when water interacts with the perovskite structure can be summarized as:

$$Sr_2Fe_{1-x}Ta_{1+x}O_6 + yH_2O \rightarrow Sr_2Fe_{1-x}Ta_{1+x}O_{6-y}(OH)_{2y}$$

The observed enhancement in radiolytic hydrogen production upon Ta substitution can be explained in terms of defect chemistry and local electronic structure modifications in the double perovskite lattice. Substitution of Fe^{3+} by Ta^{5+} modifies the charge balance and may lead to

different charge compensation mechanisms, including changes in cation valence states, B-site disorder, and possible formation of oxygen vacancies. These defects can act as active sites for water adsorption and facilitate interactions with radiolytically generated reactive species (e.g., H• and HO•). Furthermore, the d^0 electronic configuration of Ta^{5+} may contribute to improved structural stability under γ-irradiation, helping to preserve the material during the radiolytic process. However, since direct experimental evidence for defect concentrations and surface states is not available, this mechanism should be considered a literature-supported interpretation.

Experimental

The compounds were synthesized using a conventional solid-state reaction method. To optimize the synthesis conditions, the starting materials were used as fine powders and pre-dried at 120 °C for 6 h. Double perovskite-type oxides with the general formula $Sr_2Fe_{1-x}Ta_{1+x}O_6$ ($0 \leq x \leq 0.5$) were prepared from stoichiometric mixtures of high-purity $SrCO_3$, Fe_2O_3, and Ta_2O_5. The homogenized mixtures were subjected to a decarbonation treatment at 950 °C for 6 h in air using alumina crucibles. The corresponding reaction can be expressed as:

$$4\ SrCO_3 + (1-x)Fe_2O_3 + (1+x)Ta_2O_5 \rightarrow 2\ Sr_2Fe_{1-x}Ta_{1+x}O_6 + 4\ CO_2$$

The resulting powders were thoroughly ground and pressed into pellets with a diameter of 10 mm and a thickness of 2 mm under a pressure of 150 kPa. The pellets were calcined at 1100 °C for 12 h in air. After furnace cooling to room temperature, the samples were reground and re-pelletized under the same conditions to improve phase homogeneity and minimize impurity phases.

The pellets were then heat-treated at 1200 °C for 48 h with intermediate regrinding steps. After each thermal treatment, the samples were allowed to cool naturally in the furnace under ambient atmosphere. To ensure complete formation of the perovskite phase, the powders were further reground, re-pelletized, and subjected to an additional heat treatment at 1200 °C, followed by final sintering at 1300 °C for 48 h.

Phase identification was performed by X-ray diffraction (XRD), while structural characterization was complemented by Fourier-transform infrared (FT-IR) spectroscopy.

Conclusions

Polycrystalline $Sr_2Fe_{1-x}Ta_{1+x}O_6$ ($0 \leq x \leq 0.5$) double perovskites were successfully synthesized via a solid-state reaction and confirmed by XRD and FTIR to crystallize in an orthorhombic structure. Although cation substitution did not induce long-range Fe/Ta ordering, it significantly influenced both dielectric and catalytic properties. All samples exhibited normal dielectric behavior, with the $x = 0.5$ composition showing lower dielectric losses and enhanced performance. Under γ-ray irradiation during water radiolysis, the catalytic activity increased with Ta content, with the $x = 0.5$ sample exhibiting the highest hydrogen evolution. These results demonstrate that $Sr_2Fe_{1-x}Ta_{1+x}O_6$ ($0 \leq x \leq 0.5$) perovskites are promising multifunctional materials, combining favorable dielectric properties with efficient catalytic activity for hydrogen production.

Furthermore, these findings highlight the potential of cation engineering as an effective strategy for tuning the functional properties of double perovskites. Future work may focus on optimizing synthesis parameters, exploring higher substitution ranges, and investigating the underlying mechanisms governing the enhanced catalytic performance.

Conflicts of interest

The authors declare no conflicts of interest regarding this manuscript.

References

1. Anderson, M. T.; Greenwood, K. B.; Taylor, G. A.; Poeppelmeier, K.R. B-cation arrangements in double perovskites. *Prog. Solid State Chem.*,**1993**, *22*, 97 – 233. https://doi.org/10.1016/0079-6786(93)90004-B
2. Kobayashi, K. I.; Kimura, T.; Sawada, H.; Terakura, K.; Tokura, Y. Room-temperature magnetoresistance in an oxide material with an ordered double perovskite structure. *Nature* **1998**, *395*, 677 – 680. https://doi.org/10.1038/27167
3. Eng, H. W.; Barnes, P. W.; Auer, B. M.; Woodward, P.M. Investigation of the electronic structure of d^0 transition metal oxides belonging to the perovskite family. *J. Solid State Chem.* **2003**, *175*, 94 – 109. https://doi.org/10.1016/S0022-4596(03)00289-5
4. Liu, J. W.; Chen, G.; Li, Z. H.; Zhang, Z.G. Hydrothermal synthesis and photocatalytic properties of $ATaO_3$ and $ANbO_3$ (A = Na and K) *Int. J. Hydrog. Energy*, **2007**, *32*, 2269 – 2272. https://doi.org/10.1016/j.ijhydene.2006.10.005
5. Rajendran, D. N.; Nair, K. R.; Rao, P. P.; Sibi, K. S.; Koshy, P.; Vaidyan, V. K. New perovskite-type oxides: $NaATiMO_6$ (A = Ca or Sr; M = Nb or Ta) and their electrical properties. *Mater. Lett.*, **2007**, *62*, 623 – 628. https://doi.org/10.1016/j.matlet.2007.06.022
6. Holman, K. L.; Huang, Q.; Klimczuk, T.; Trzebiatowski, K.; Bos, J. W. G.; Morosan, E.; Lynn, J. W.; Cava, R. J. Synthesis and properties of the double perovskites La_2NiVO_6, La_2CoVO_6, and La_2CoTiO_6. *J. Solid State Chem*. **2007**, *180*, 75 – 83. https://doi.org/10.1016/j.jssc.2006.09.013
7. Takahashi, Y.; Nakajima, Y.; Morishita, T.; Tanabe, K. Effects of oxygen pressure in preparation of insulating Sr_2AlTaO_6 thin films by MOCVD. *Physica C: Supercond.Appl.*, **2002**, *378–381*, 1357 – 1361. https://doi.org/10.1016/S0921-4534(02)01714-8.
8. Kudo, A.; Kato, H.; Nakagawa, S. Water splitting into H_2 and O_2 on new $Sr_2M_2O_7$ (M = Nb and Ta) photocatalysts with layered perovskite structures: Factors affecting the photocatalytic activity. *J. Phys. Chem. B* **2000**, *104*, 571 – 575. https://doi.org/10.1021/jp9919056

9. Gorodea, I.; Goanta, M.; Toma, M. Impact of A cation size of double perovskite A_2AlTaO_6 (A = Ca, Sr, Ba) on dielectric and catalytic properties. *J. Alloys Compd.* **2015**, *632*, 805 – 809. https://doi.org/10.1016/j.jallcom.2015.01.310
10. Lufaso, M. W.; Woodward, P. M. Prediction of the crystal structures of perovskites using the software program SPuDS. *Acta Crystallogr. B* **2001**, *57*, 725 – 738. https://doi.org/10.1107/S0108768101015282
11. Chakraverty, S.; Saito, M.; Tsukimoto, S.; Ikuhara, Y.; Ohtomo, A.; Kawasaki, M. Magnetic properties of Sr_2FeTaO_6 double perovskite epitaxially grown by pulsed-laser deposition. *Appl. Phys. Lett.* **2011**, *99*, 222901. https://doi.org/10.1063/1.3663214
12. Lavat, A. E.; Baran, E. J. IR-spectroscopic characterization of $A_2BB'O_6$ perovskites. *Vib. Spectrosc.* **2003**, *32*, 167 – 174. https://doi.org/10.1016/S0924-2031(03)00059-6
13. Maxwell, J. C. A Treatise on Electricity and Magnetism; Cambridge University Press: Cambridge, UK, **2010**; ISBN 978-1108014045.
14. Baker, J.; Geyer, R. G.; Grosvenor, J. H.; Janezic, M. D.; Jones, C. A.; Riddle, B.; Weil, C. M.; Krupka, J. Dielectric characterization of low-loss materials: A comparison of techniques. *IEEE Trans. Dielectr. Electr. Insul.* **1998**, *5*, 571 – 577. https://doi.org/10.1109/94.708274
15. Rajmi, R.; Maulud, M.F.; Mohamed, Z. Structural, optical and dielectric properties of tellurium-based double perovskite $Sr_2Ni_{1-x}Zn_xTeO_6$. *RSC Adv.* **2021**, *11*, 31631. https://doi.org/10.1039/D1RA03662A
16. Oliveira, F. S.; Santos, C. A. M.; Machado, A. J. S.; Banerjee, P.; Franco, A. Structure and dielectric properties of BaCuYTaO double perovskite. *SN Appl. Sci.* **2019**, *1*, 1447. https://doi.org/10.1007/s42452-019-1479-z
17. Abe, R. Development of a new system for photocatalytic water splitting into H_2 and O_2 under visible light irradiation. *Bull. Chem. Soc. Jpn.* **2011**, *84*, 1000 – 1030. https://doi.org/10.1246/bcsj.20110132
18. Li, D.; Zheng, J.; Zou, Z. Band structure and photocatalytic properties of perovskite-type compound Ca_2NiWO_6 for water splitting. *J. Phys. Chem. Solids* **2006**, *67*, 801 – 806. https://doi.org/10.1016/j.jpcs.2005.10.182
19. Zhu, Y.; Zhang, L.; Zhao, B.; Chen, H.; Liu, X.; Zhao, R.; Wang, X.; Liu, J.; Chen, Y.; Liu, M. Improving the Activity for Oxygen Evolution

Reaction by Tailoring Oxygen Defects in Double Perovskite Oxides. *Adv. Funct. Mater*. **2019**, *29*, 1901783. https://doi.org/10.1002/adfm.201901783

20. Grimaud, A.; May, K. J.; Carlton, C. E.; Hong, W. T.; Lee, Y. L.; Risch, M.; Stoerzinger, K. A.; Shao-Horn, Y. Double perovskites as a family of highly active catalysts for oxygen evolution in alkaline solution. *Nat. Commun*. **2013**, *4*, 2439. https://doi.org/10.1038/ncomms3439